Vol 13 No 9, September 2004
1009-1963/2004/13(09)/1544-05

Chinese Physics

© 2004 Chin. Phys. Soc.
and IOP Publishing Ltd

Dynamic dc voltage band in vertical transport of superlattices*

Wu Bin-Yi(吴彬毅)†, Duan Su-Qing(段素青), and Zhao Xian-Geng(赵宪庚)

Institute of Applied Physics and Computational Mathematics, Beijing 100088, *China*

(Received 20 February 2004; revised manuscript received 30 April 2004)

By the numerical method, we show a transition process from static to dynamic electric-field domain formation in semiconductor superlattices. During this transition, there can be noticed a sawtooth-like zone in which static and dynamic electric-field domain zones appear alternatively with increasing voltage. Therefore, a dynamic dc voltage band emerges from each sawtooth-like branch of the current–voltage characteristic. These results are qualitatively in agreement with experiment.

Keywords: dynamic dc voltage band, phase diagram, sawtooth-like zone, semiconductor superlattices
PACC: 7355, 7340L

1. Introduction

Some features that are associated with vertical transport in strongly coupled superlattices, such as Bloch oscillation, dynamical localization, and miniband transport, have been widely discussed with a tight-binding model.[1−4] For the superlattices with larger barrier widths, the coupling is weaker, and sequential tunnelling of electrons between different wells plays a dominant role in the charge carrier transport in the system. In the past years, depending upon the circuit conditions and the material parameters, e.g. the mean doping density $N_{\rm D}$, either stable stationary domains (for high $N_{\rm D}$), or self-sustained oscillation of the domains (for intermediate $N_{\rm D}$) are found in weakly coupled superlattice (SL).[5−10] It has been shown that the current self-sustained oscillation only occurs within a certain range of carrier concentration. However, above this carrier concentration range the current–voltage ($I-U$) characteristics exhibit discontinuities on the sequential resonance tunnelling (SRT) plateau and show a series of sawtooth-like current branches corresponding to the static electric-field domain (EFD) formation.[5,11] So, we know that changing of $N_{\rm D}$ will lead to a transition between the static and dynamic formations of EFD. The same transition can be produced by applying an external magnetic field parallel to the SL layers [12] or increasing the sample temperature. The SL sample temperature induced transition process between the static and dynamic formations of EFD has been investigated in detail, in which a phenomenon is observed: a dynamic dc voltage band is found emerging from each sawtooth-like branch of the $I-U$ characteristic in experiment. As temperature increases, dynamic dc voltage bands appear and expand within each sawtooth-like branch, squeeze out the static region, and join together to turn the whole plateau into a dynamic EFD formation from the static one.[13]

On the theoretical side, it has been shown that the $I-U$ characteristic and dynamic dc voltage band can be reproduced fairly well by the models which combine essentially the discrete Poisson equation and rate equations for carrier densities in the different quantum wells.[14−16]

In this paper, the transition process between static and dynamic formations of EFD is produced by the numerical method in SL, and the dynamic dc voltage band is investigated in detail.

2. Model

Consider a SL of N wells, the state of SL is de-

*Project supported in part by the National Natural Science Foundation of China (Grant Nos 10274007 and 90103027), and a Grant of the China Academy of Engineering Physics.
†Corresponding author: wbyfuture@hotmail.com

scribed by the electric field E_i on the ith barrier, where $i = 1, 2, \ldots, N$ is the barrier index. Deviations of electron densities in the wells from the doping density $N_{\rm D}$ cause an inhomogeneous field distribution via the discrete Poisson equations

$$\epsilon(E_i - E_{i-1}) = ed(n_i - N_{\rm D}), i = 1, 2, \ldots, N, \quad (1)$$

where n_i is the electron density in the ith well, e is the electron charge, d is the period of SL, and ϵ is the permittivity. The fields have to satisfy the global voltage constraint

$$U = \sum_{i=1}^{N} E_i d, \quad (2)$$

where U is the bias voltage. Ampère's equation for the balance of current densities

$$\epsilon \frac{{\rm d}E_i}{{\rm d}t} + en_i v(E_i) = J, i = 1, 2, \ldots, N, \quad (3)$$

where $v(E_i)$ is a drift velocity for the local voltage drop, and J is the total current densities. The boundary condition [17] is

$$n_0 = (1 + C)N_{\rm D}, \quad (4)$$

where C is a quite small dimensionless value. According to the transport characteristic of SRT, we select the sum of two *Lorentzian* functions as the phenomenological drift velocity.[13]

$$\frac{v(E_i)}{v(E_M)} = \left(\frac{0.81{\rm WQ}_1}{\left(\frac{E_i}{E_M} - 1.0\right)^2 + {\rm WQ}_1} + \frac{2{\rm WQ}_2}{\left(\frac{E_i}{E_M} - 2.35\right)^2 + {\rm WQ}_2} \right), \quad (5)$$

where ${\rm WQ}_1$, ${\rm WQ}_2$ are the dimensionless parameters of *Lorentzian* drift velocity.

As shown in Fig.1, under field $E_{\rm M}$, the SRT relates the first level of the ith well and the second level of the $(i+1)$th well, and under field $E_{\rm M1}$ the SRT may relate the first level of the ith well and the third level of the $(i+1)$th well, or the second level of the ith well and the third level of the $(i+1)$th well, which determine the different subband energy structures. We set our Eqs.(1)–(5) dimensionless by using the characteristic physical quantities as follows. We take $E_{\rm M}$ as the unit for electric field E, where $E_{\rm M}=\Delta/(ed)$, with Δ being the energy separation between the first and the second electron subbands. The unit of $v(E)$ is its value at $E = E_{\rm M}$, where it has a local maximum due to resonance in tunnelling. Then, we take J_0 (where $J_0 = \epsilon v(E_{\rm M})/d$), U_0 (where $U_0 = NE_{\rm M}d$), $N_{\rm D0}$ (where $N_{\rm D0}$ is defined as $\epsilon E_{\rm M}/ed$), and $t_{\rm tun}$ (where $t_{\rm tun}=d/v(E_{\rm M})$) as units of J, U, $N_{\rm D}$, t, respectively. The system is solved numerically by the fourth-order Runge–Kutta method. When simulating the $I - U$ characteristic by increasing dc bias U, we use a uniform initial field profile at the lattices in low dc bias. In the step of next dc bias, the initial field profile is determined by the distribution of long-time mean value of $E_i(t)$ which is the calculated result of last dc bias.

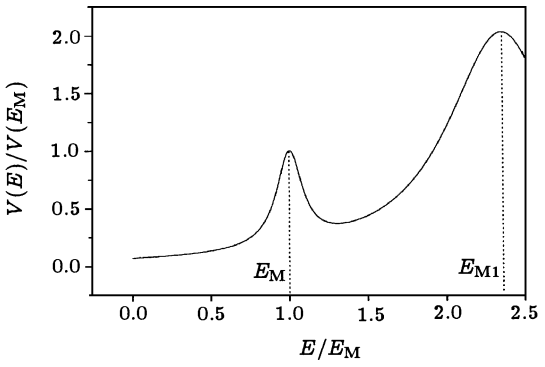


Fig.1. Velocity of the electrons as a function of the electric field, for the fixed parameters ${\rm WQ}_1 = 0.01$ and ${\rm WQ}_2 = 0.18$. $E_{\rm M}$, $v(E_{\rm M})$ are taken as the units of electric field E and drift velocity $v(E)$, respectively. $E_{\rm M}$ and $E_{\rm M1}$ are the locations of two sequential resonant tunnelling peaks.

3. Results and discussion

The typical phase diagrams which distinguish the dynamic zone (current self-oscillation zone) from the static zone (non-oscillating zone) are shown in Fig.2 for fixed ${\rm WQ}_1 = 0.01$, $N = 40$, ${\rm WQ}_2 = 0.18$, $C = 0.001$; and in Fig.3 for fixed $N_{\rm D} = 0.13$, $N = 40$, ${\rm WQ}_2 = 0.18$, $C = 0.001$. The value of the iso-amplitude line denotes the oscillation amplitude of $J(t)$. At the top zone of Fig.2 and bottom zone of Fig.3, we can notice a sawtooth-like zone in which the static and dynamic zones appear alternatively with increasing voltage. Here, we can obtain dynamic dc voltage bands by computing current–voltage curves of the above zones.

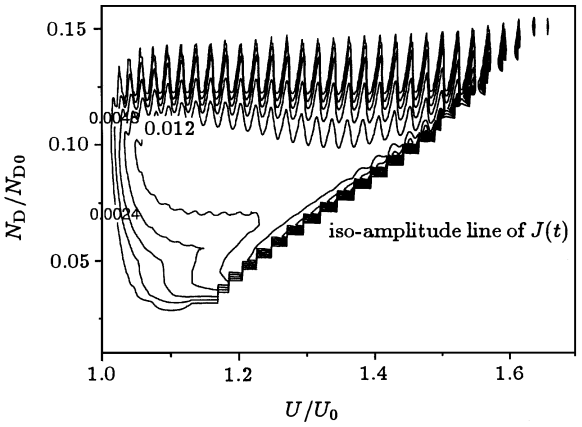


Fig.2. A phase diagram of the amplitude of self-oscillation current $J(t)$ as a function of the mean doping density N_D and voltage U for the fixed dimensionless parameters $WQ_1 = 0.01$ of a semiconductive SL. The value of iso-amplitude line denotes the amplitude of $J(t)$. Here, $N = 40$, $WQ_2 = 0.18$, $C = 0.001$.

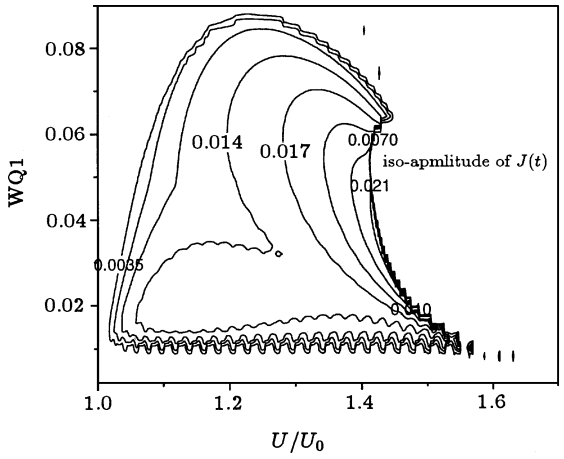


Fig.3. A phase diagram of the amplitude of self-oscillation current $J(t)$ as a function of the dimensionless parameter WQ_1 and voltage U for fixed $N_D = 0.13$ of a semiconductive SL. the value of the iso-amplitude denotes the amplitude of $J(t)$. Here, $N = 40$, $WQ_2 = 0.18$, $C = 0.001$.

How to simulate the experimental results in Ref.[9]? Figure 2 shows that a transition from dynamic to static EFD occurs, as N_D increases in the range from N_D=0.10 to 0.15, for fixed WQ_1=0.01. In this transition, we can find that the dynamic dc voltage bands appear and expand, within each sawtooth-like branch of the $I - U$ characteristic, squeeze out the static region, and join together to turn the whole plateau into a dynamic electric-field domain formed from the static field domain. In the model, we know that average carrier concentration is not equivalent to average doping density at about 100K because impurity excitation is not complete (intrinsic exciting is neglected). So, increasing temperature will lead to a little increase of carrier concentration in the SL. This process could be simulated by the increase of the parameter N_D of the model. However, it is shown in Fig.2 that the transition occurring with increasing N_D is a reversal process of the transition from static to dynamic EFD induced by increasing temperature, which has been found in Ref.[9].

For the simulation of experimental results, we consider another factor, the width of resonant tunnelling peak, which will be broadened with increasing temperature. This corresponds to the result of raising the value of WQ_1 in our model. Naturally, we focus on the transition for fixed N_D, which occurs by changing WQ_1 in the range of $WQ_1 \approx 0.005$ to 0.02, as shown in Fig.3. This shows that the transition occurring by increasing WQ_1 is in qualitative agreement with the experimental result. We draw a group of $I-U$ curves to simulate the experimental results, but these $I-U$ curves overlap for a fixed N_D because the value of N_D is related positively to the mean current density J. Obviously, the experimental result shows that raising temperature will result in a little increase of carrier concentration. Hence, the result of increasing temperature should be simulated by simultaneously increasing N_D and WQ_1 of our model (see Fig.5, the values of WQ_1 and N_D at a certain temperature is related to the material quality). However, the two cases, solely increasing the value of WQ_1 or N_D in our model, will lead to two reversal transition processes, as shown in Figs.2 and 3. Could we simulate experimental results by synthesizing the two factors? Fortunately, we obtain a group of $I - U$ curves by the numerical method, which is shown in Fig.4. (similar to the Fig.2 of Ref.[9]) It is in good agreement with the experimental result. In this case, the transition from static to dynamic EFD caused by increasing WQ_1 is dominant in the procedure of increasing temperature, and a reversal process with increasing N_D is counteracted.

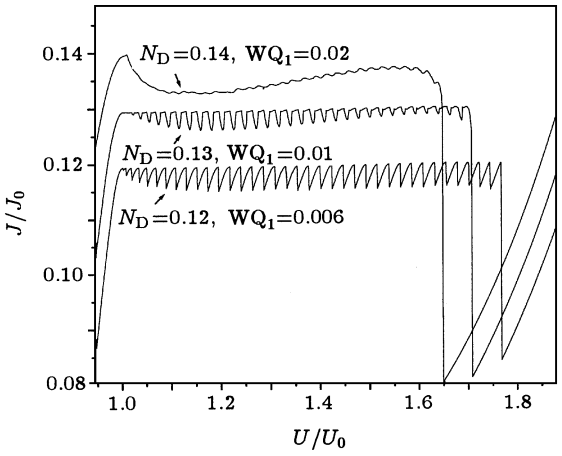


Fig.4. From bottom up, $I-U$ curves showing a transition process from static to dynamic EFD caused by simultaneously increasing N_D and WQ_1. Here $N = 40$, $WQ_2 = 0.18$, $C = 0.001$; bottom curve: N_D=0.12, $WQ_1 = 0.006$, immediate curve: N_D=0.13, $WQ_1 = 0.01$ and top curve: N_D=0.14, $WQ_1 = 0.02$.

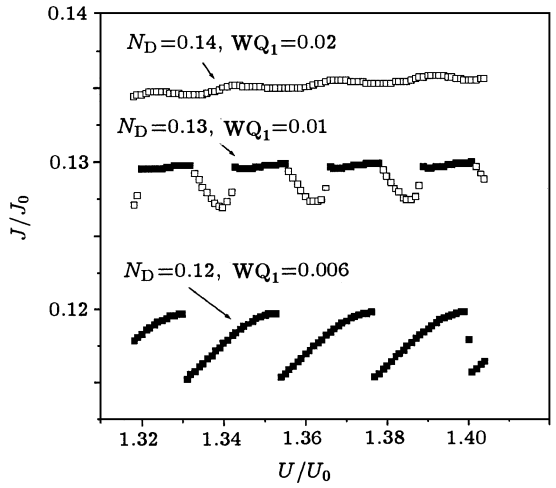


Fig.5. Enlargement of Fig.4. The dynamic voltage band emerges at each current branch. Open squares indicate the dynamic region while solid squares indicate the static region.

For investigating this transition, we focus on these $I-U$ curves, shown in Fig.4. Here, J is mean current density. They exhibit a series of about 40 sawtooth-like current branches. One sawtooth-like current branch represents a well jumping from low-field to high-field. In the right plateau, currents fall sharply. It presents the last several wells jumping to high field simultaneously because of instability. Hence, when parameter $N = 40$, the number of sawtooth-like current branches of these $I-U$ curves will be less than 40. The same phenomenon has been found in Ref.[9]. In Fig.4, it can be noticed that a transition from static to dynamic EFD occurs. For N_D=0.12, $WQ_1 = 0.006$, the bottom curve exhibits a series of sawtooth-like current branches which correspond to the static EFD. For N_D=0.14, $WQ_1 = 0.02$, in the top curve the sawtooth-like branches disappear, a flat current plateau is observed, and the current self-oscillations appear under dc biases across the whole plateau, indicating the dynamic EFD formation. When N_D=0.13, $WQ_1 = 0.01$, namely, the intermediate curve, we see the dynamic dc voltage bands emerge from each sawtooth-like current branch. In these bands, current self-oscillations are observed. As is more clearly shown, an enlargement of Fig.4 in detail is in Fig.5 (similar to Fig.3 of Ref.[9]). Open squares indicate the dynamic region while solid squares indicate the static region. Figure 6 (similar to Fig.4 of Ref.[9]) shows an example of the temporal current self-oscillation with N_D=0.13, $WQ_1 = 0.01$ and applied dc bias $U = 1.358$ within a dynamic voltage band.

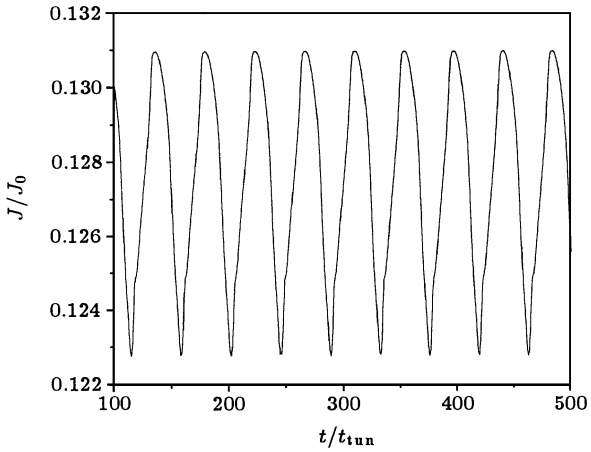


Fig.6. Simulated periodic time dependence of the current at N_D=0.13, $WQ_1 = 0.01$, and $U = 1.358$. showing the so-called current self-oscillation or dynamic EFD.

In summary, by the numerical method, we have drawn two phase diagrams in which the sawtooth-like zones show that the static and dynamic EFD zones appear alternatively with increasing voltage in vertical transport of SL. Therefore, a dynamic dc voltage band emerges from each sawtooth-like branch of the current–voltage characteristic. Under the guidance of the phase diagrams, we can obtain transition processes between the static and dynamic formations of EFD by solely changing WQ_1 or N_D. However, the SL sample temperature induced transition process is simulated by simultaneously changing the two factors. These results are qualitatively in agreement with the experiment results.

References

[1] Zhao X G 1991 *Phys. Lett.* A **155** 299
Zhao X G 1994 *Phys. J: Condens. Matter* **6** 2751

[2] Zhao X G, Georgakis G A and Niu Q 1996 *Phys. Rev.* B **54** R5235
Zhao X G, Georgakis G A and Niu Q 1997 *Phys. Rev.* B **56** 3976

[3] Duan S Q and Zhao X G 2000 *Phys. Rev.* B **61** 5442

[4] Duan S Q, Wang Z G and Zhao X G 2003 *Chin. Phys.* **12** 8

[5] Chang L L, Esaki L and Tsu R 1974 *Appl. Phys. Lett.* **24** 593
Esaki L and Chang L L 1974 *Phys. Rev. Lett.* **8** 496

[6] Merlin R, Kwok S H, Norris T B, Grahn H T, Ploog K, Bonilla L L, Galan J, Cuesta J A, Martinez F C and Moleara J 1995 in *Proceedings of the 22nd International Conference on the Physics of Semiconductors* (Singapore: World Scientific) Vol.**2** p1039

[7] Grahn H T, Kastrup J, Ploog K, Bonilla L L, Galan J, Kindelan M and Moscoso M 1995 *Jpn. J. Appl. Phys.* Part 1 **34** 4526

[8] Kastrup J, Hey R, Ploog K H, Grahn H T, Bonilla L L, Kindelan M, Moscoso M, Wacker A and Galan J 1997 *Phys. Rev.* B **55** 2476

[9] Ohtani N, Egami N, Grahn H T, Ploog K and Bonilla L L 1998 *Phys. Rev.* B **58** R7528

[10] Sun B, Jiang D and Wang X 1997 *Semicond. Sci. Technol.* **12** 401

[11] Grahn H T, Hang R J, Muller W and Ploog K 1991 *Phys. Rev. Lett.* **67** 1618

[12] Sun B, Wang J, Ge W, Wang Y, Jiang D, Wang H, Deng Y and Feng S 1999 *Phys. Rev.* B **60** 8866

[13] Wang J, Sun B, Wang X, Wang Y, Ge W and Wang H 1999 *Appl. Phys. Lett.* **75** 2620

[14] Prengel F, Wacker A and Shröll E 1994 *Phys. Rev.* B **50** 1705
Prengel F, Wacker A and Shröll E 1995 *Phys. Rev.* B **52** 11518

[15] Bonilla L L, Galan J, Cuesta J A, Martinez F C and Molera J M 1994 *Phys. Rev.* B **50** 8644

[16] Miller D and Laikhtman B 1994 *Phys. Rev.* B **50** 18426

[17] Wacker A, Moscoso M, Kindelan M and Bonilla L L 1997 *Phys. Rev.* B **55** 2466